Better Software or Hardware for Analyzing Sound Sources?

Sean Wu
Department of Mechanical Engineering
Wayne State University
Detroit, MI 48202
U.S.A.

Yazhong Lu
Signal-Wise, LLC
Troy, Michigan 49084
U.S.A.

Cheng-Hsiang Kuo, Jin-lian Chen, Tsai-Tsan Yao, Jack Lee, Vickie Wu and Sam Wu
Samwell Testing Inc.
Taipei, Taiwan

Abstract

In tackling challenging noise and vibration problems, a natural tendency is steered toward having better and more sensors, hoping that this will offer more information about the target sources and insight into the underlying principle of noise and vibration problems. This paper demonstrates that developing a better technology is more effective than relying on more hardware. Specifically, this paper presents a methodology that will enable one to acquire comprehensive knowledge of sound sources locations, sound pressure distributions, and sound intensities or energy flows from sound sources to the surrounding three-dimensional fluid medium. In particular, this method allows one to correlate five physical quantities that include time, space, frequency, visual and hearing effects resulting from the captured target sources. It is shown that all these tasks can be accomplished by using six microphones. The underlying principle involved in this technology is a hybrid approach that combines the time delay of arrival for blind source localization and acoustical holography for visualizing the sound field in 3D space. The former enables one to pinpoint the exact locations of a large number of sound sources simultaneously, and the latter allows for reconstructing the sound pressure fields generated by the sound sources in three-dimensional space and the flow of acoustic

energy from source surfaces. Examples of using this technology to gain a better understanding of the time-space-frequency-visual-hearing correlations of complex sources are demonstrated.

I. Introduction

Noise has always been one of the major concerns facing the manufacturers of automobile, aircraft, consumer appliances, consumer electronics, ship, etc. The first step toward noise control is to locate noise sources and analyze the source characteristics. Currently, a common technology for locating noise sources is to use beamforming,[1, 2, 3, 4] whose algorithm is built on the delay-and-sum principle, namely, the signals measured by microphones are delayed systematically until they are all in phase. This is equivalent to rotating the sensor array till the incident sound wave reaches all sensors simultaneously. The bearing of any sound wave can be specified because the amplitude of the acoustic pressure is maximal in the direction of wave propagation, which forms a beam and its name. However, beamforming cannot tell the source range and its spatial resolution is limited to one wavelength of the sound emitted by a source. Moreover, beamforming is two-dimensional, cannot provide the source level, and cannot reveal the radiation pattern of a sound source. As such, beamforming can only offer a qualitative image of a source location, which is not enough to yield a good insight of the whereabouts of noise sources, not to mention their characteristics. Another shortcoming is due to the fact that beamforming requires a large number of sensors, which raises the overall costs of noise diagnosis and mitigation.

In this paper a new technology known as TSF V-Sonics (Time-Space-Frequency Visual and Sound) is presented for noise diagnosis and analysis. As its name suggests, TSF V-Sonics enables one to locate a large number of sound sources, much larger than the number of sensors included, in an arbitrary three-dimensional (3D) space simultaneously. Most importantly, it enables the users to acquire the time-space-frequency-visual-sound correlations of target noise sources at a narrow frequency band and small time step, locate exactly where sound is emitted in 3D space, visualize

sound pressure distributions in terms of SPL values on the source surface and in 3D space, and 3D sound intensity vector distributions on the source surface in a narrow- or broad-band and in small time steps. All these features and functions of TSF V-Sonics can be obtained by using six sensors.

II. Theory

It is emphasized that TSF V-Sonics is developed to solve real noise diagnosis and analysis problems that may be encountered in engineering practice. In almost all engineering applications, the test environment is non-ideal, namely, the surrounding is not free field, the boundary surfaces and obstacles that may cause sound reflections and reverberation are unknown a priori. Therefore, there is no way of finding an analytic solution to the sound field that is generated by an unknown number of sound sources inside an unspecified environment. With this in mind, it is unrealistic to expect TSF V-Sonics to provide exact sound source locations, SPL values on the source surfaces as well as in 3D space, and the intensity vector distributions on the source surface at any narrow- or broad-band frequencies and small time steps.

What TSF V-Sonics attempts to offer is the optimal approximations to questions in hand. Theoretically TSF V-Sonics is based on two main technologies for blind sound source localization and reconstruction of the sound field emitted by an arbitrary number of sources in 3D space. The former is called passive SODAR (Sonic Detection And Ranging),[5, 6, 7] whose underlying principles are TDOA (Time Difference Of Arrival) and triangulations to locate the Cartesian coordinates of a target sound source in 3D space. The latter is known as HELS (Helmholtz Equation Least Squares) based NAH (Nearfield Acoustical Holography),[8, 9, 10, 11, 12] which has been utilized to analyze the airborne and structure-borne acoustic fields generated by various complex vibrating structures in engineering applications.

Mathematically, passive SODAR for blind sound source localization can be written as the following triangulation formula,

$$\sqrt{\left(x-x_i\right)^2+\left(y-y_i\right)^2+\left(z-z_i\right)^2}=\sqrt{\left(x-x_1\right)^2+\left(y-y_1\right)^2+\left(z-z_1\right)^2}+\left(c\Delta t_{1,i}\right),\ i=2,3,\cdots 6;\ (1)$$

where (x, y, z) depict the Cartesian coordinates of the source, (x_i, y_i, z_i), $i = 1, 2, \cdots, 6$, are those of the sensors that are specified in the design of the sensor array, Δt_{1i}, $i = 2, 3, \cdots, 6$, implies the time delays between the 1st and i^{th} sensor, respectively, which are obtained by taking cross correlations between individual pairs of sensors.

Analytic solution to Eq. (1) is presented in References 5 to 6 and omitted for brevity in this paper. It is emphasized that there are no restrictions whatsoever on the locations of a target sound source and sensors. In other words, the analytic solution (1) for locating the Cartesian coordinates of any source is valid in 3D space, so long as sensors do not all lie on the same plane. This property provides users the greatest flexibility in practice to suit any test site to achieve the optimal source localization results in the most cost-effective manner. Needless to say, the line of sight among all sensors must constantly be kept unblocked.

Reconstruction of the acoustic pressure field generated by the captured sound source in 3D space as well as the acoustic intensity vector distribution on the source surface can be obtained by using the HELS method. Mathematically, the reconstructed acoustic quantities are expressible as,

$$\left\{\hat{p}\left(\vec{x};\omega\right)\right\}_{N\times 1}=\left[G_{pp}\left(\vec{x}\middle|\vec{x}_m;\omega\right)\right]_{N\times M}\ \left\{\hat{p}\left(\vec{x}_m;\omega\right)\right\}_{M\times 1},\qquad(2)$$

$$\left\{\hat{v}_n\left(\vec{x};\omega\right)\right\}_{N\times 1}=\left[G_{vp}\left(\vec{x}\middle|\vec{x}_m;\omega\right)\right]_{N\times M}\ \left\{\hat{p}\left(\vec{x}_m;\omega\right)\right\}_{M\times 1},\qquad(3)$$

where $\left\{\hat{p}\left(\vec{x};\omega\right)\right\}_{N\times 1}$ and $\left\{\hat{v}_n\left(\vec{x};\omega\right)\right\}_{N\times 1}$ represent the column vectors of the reconstructed acoustic pressure and normal component of the particle velocity, respectively, at any desired location $\vec{x}$ in 3D space including the source surface, $\left\{\hat{p}\left(\vec{x}_m;\omega\right)\right\}_{M\times 1}$ depicts the column vector containing the acoustic pressure measured on a hologram surface, $\vec{x}_m$, $m = 1, 2, \cdots, M$, $\left[G_{pp}\left(\vec{x}\middle|\vec{x}_m;\omega\right)\right]_{N\times M}$ and

$\left[G_{vp}\left(\vec{x}\middle|\vec{x}_m;\omega\right)\right]_{N\times M}$ are the transfer matrices that correlate the measured pressure $\left\{\hat{p}\left(\vec{x}_m;\omega\right)\right\}_{M\times 1}$ on a hologram surface to the reconstructed acoustic pressure $\left\{\hat{p}\left(\vec{x};\omega\right)\right\}_{N\times 1}$ and normal component of the particle velocity $\left\{\hat{v}_n\left(\vec{x};\omega\right)\right\}_{N\times 1}$, respectively,

$$\left[G_{pp}\left(\vec{x}\middle|\vec{x}_m;\omega\right)\right]_{N\times M}=\left[\Psi\left(\vec{x};\omega\right)\right]_{N\times M}\left[\Psi\left(\vec{x}_m;\omega\right)\right]^{\dagger}_{M\times M}, \tag{4}$$

$$\left[G_{vp}\left(\vec{x}\middle|\vec{x}_m;\omega\right)\right]_{N\times M}=\frac{1}{i\omega\rho_0}\left[\nabla\Psi\left(\vec{x};\omega\right)\cdot\vec{\mathrm{n}}\right]_{N\times M}\left[\Psi\left(\vec{x}_m;\omega\right)\right]^{\dagger}_{M\times M}, \tag{5}$$

where $\vec{\mathrm{n}}$ is the unit normal vector at $\vec{x}$ and $\left[\Psi\left(\vec{x}_m;\omega\right)\right]^{\dagger}_{M\times M}$ is a pseudo inversion defined as,

$$\left[\Psi\left(\vec{x}_m;\omega\right)\right]^{\dagger}_{M\times M}=\left(\left[\Psi\left(\vec{x}_m;\omega\right)\right]^{H}_{M\times M}\left[\Psi\left(\vec{x}_m;\omega\right)\right]_{M\times M}\right)^{-1}\left[\Psi\left(\vec{x}_m;\omega\right)\right]^{H}_{M\times M}, \tag{6}$$

where the superscript *H* implies a conjugate transposition of a matrix $\left[\Psi\left(\vec{x};\omega\right)\right]$, whose elements are the particular solution to the Helmholtz equation and expressible in spherical coordinates as

$$\Psi_j\left(r,\theta,\phi;\omega\right)\equiv\Psi_{nl}\left(r,\theta,\phi;\omega\right)=h_n^{(1)}\left(kr\right)Y_n^l\left(\theta,\phi\right), \tag{7}$$

where $h_n^{(1)}\left(kr\right)$ and $Y_n^l\left(\theta,\phi\right)$ represent, respectively, the spherical Hankel functions of the first kind and the spherical harmonics, and the indices *j*, *n* and *l* in Eq. (7) are related through the following relationship, $j = n^2 + n + l + 1$, with *n* ranging from 0 to *N* and *l* from $-n$ to $+n$, where *N* indicates the number of the reconstruction points in space and on a source surface.

Equations (2) and (3) offer approximate solutions to the reconstructed acoustic quantities, based on the information collected on a hologram surface at $\vec{x}_m$. It is emphasized that the HELS method always attempts to yield the best approximations for any given set of input data by using an optimization process. Therefore the more accurate the input data are, the better the approximate reconstruction results become.

III. Test Setup

Figure 1 exhibits the hardware of TSF V-Sonics, which includes: 1) Six free-field probe microphones; 2) Two four-channel cDAQ by National Instruments; 3) One 3D scanner; 4) One viewing screen; 5) One web camera; 6) One laptop computer; 7) One tripod; and 8) One dolly.

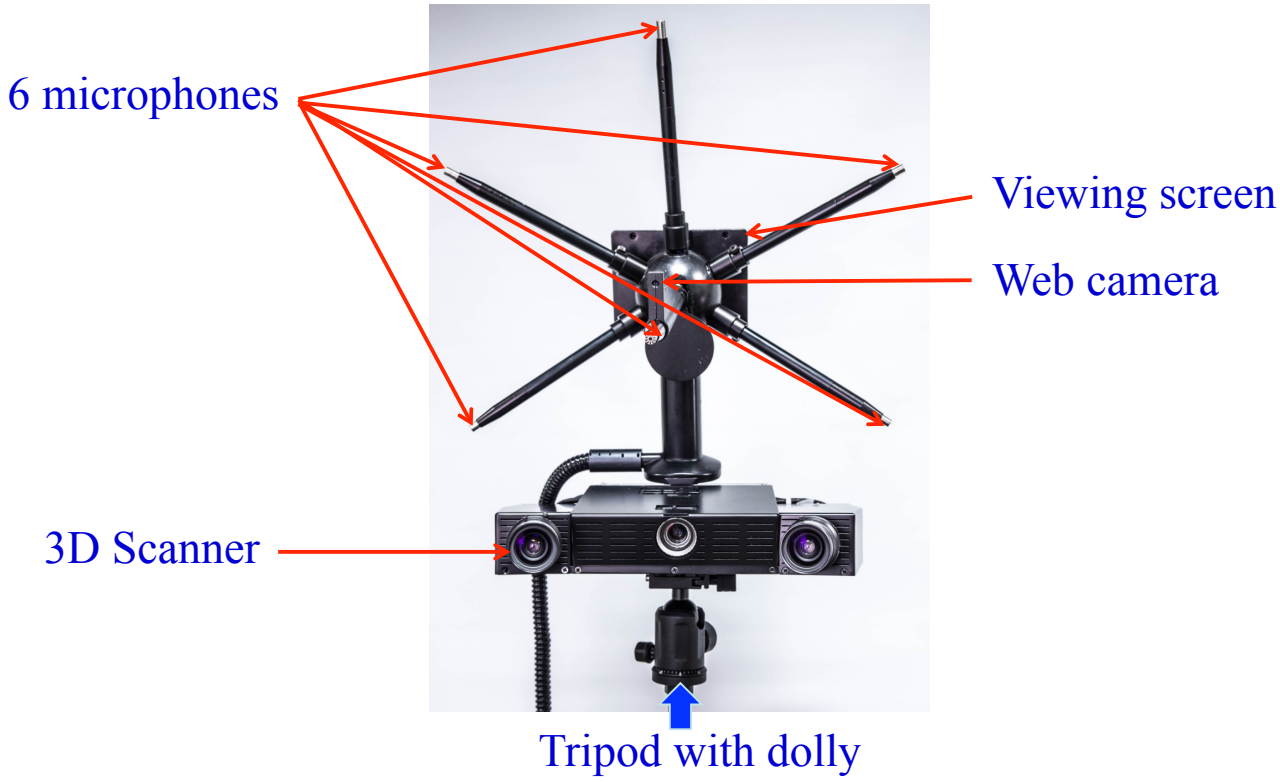

Figure 1. The major hardware involved in TSF V-Sonics include: 1) Six free-field probe microphones; 2) Two four-channel cDAQ by National Instruments; 3) One 3D scanner; 4) One viewing screen; 5) One web camera; 6) One laptop computer; 7) One tripod; and 8) One dolly.

To examine the effectiveness of using TSF V-Sonics to locating complex sound sources and analyzing the resultant sound field inside non-ideal environment, we selected a regular office setting, which contained furniture, protruding objects and boundary surfaces with vastly different acoustic absorption coefficients and with people walking by and talking as usual. The reason for selecting such a non-ideal test condition is to prepare for the worst-case scenario in applications.

Figure 2 shows a specific test setup that involved a loudspeaker. The reason for choosing this speaker was that the sound source was well defined. This would facilitate validations of using TSF V-Sonics to locate the sound source in highly non-ideal test environment, and analyzing the characteristics of the resultant sound field.

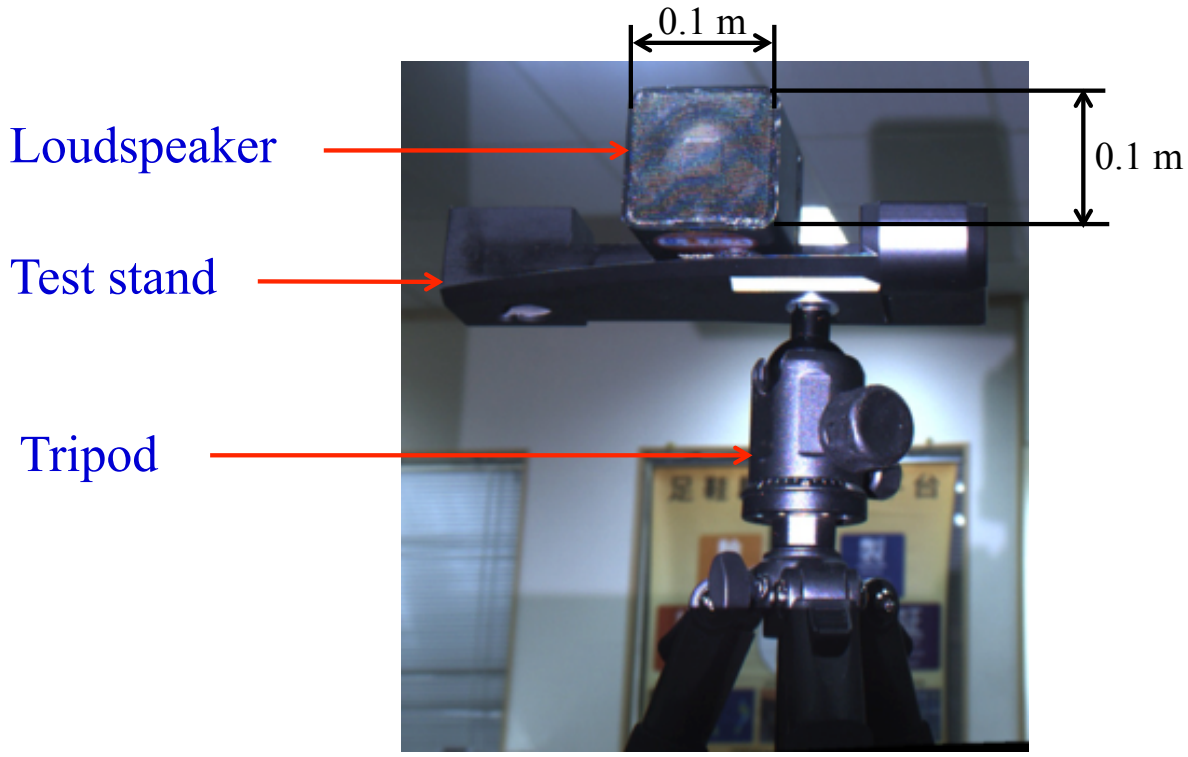

Figure 2. The test setup for a loudspeaker inside a typical office. The dimensions of this speaker were 0.1 by 0.1 by 0.1 m^3.

Once the functionalities of using TSF V-Sonics to locate a well defined sound source and analyzing the corresponding sound fields were completed, we proceeded to a much more complex sound source and field, namely, an aerodynamically generated sound field from a household hair dryer in highly non-ideal test environment (see Figure 3).

The reason to test the functionalities of using TSF V-Sonics for locating and analyzing the aerodynamically generated sound source and field is that currently there are no effective methods to perform such tasks, yet the demand on understanding aerodynamically generated sound is huge.

It is emphasized that in this study we choose to conduct the tests under a highly non-ideal condition to examine the effectiveness of TSF V-Sonics technologies in diagnosing and analyzing various noise issues. Better results could have been obtained, had the tests been conducted inside an anechoic chamber. However, in engineering applications most test conditions are non-ideal. So these studies will have a significant impact for TSF V-Sonics to become the method of choice for engineers to tackle a variety of challenging noise problems in the future.

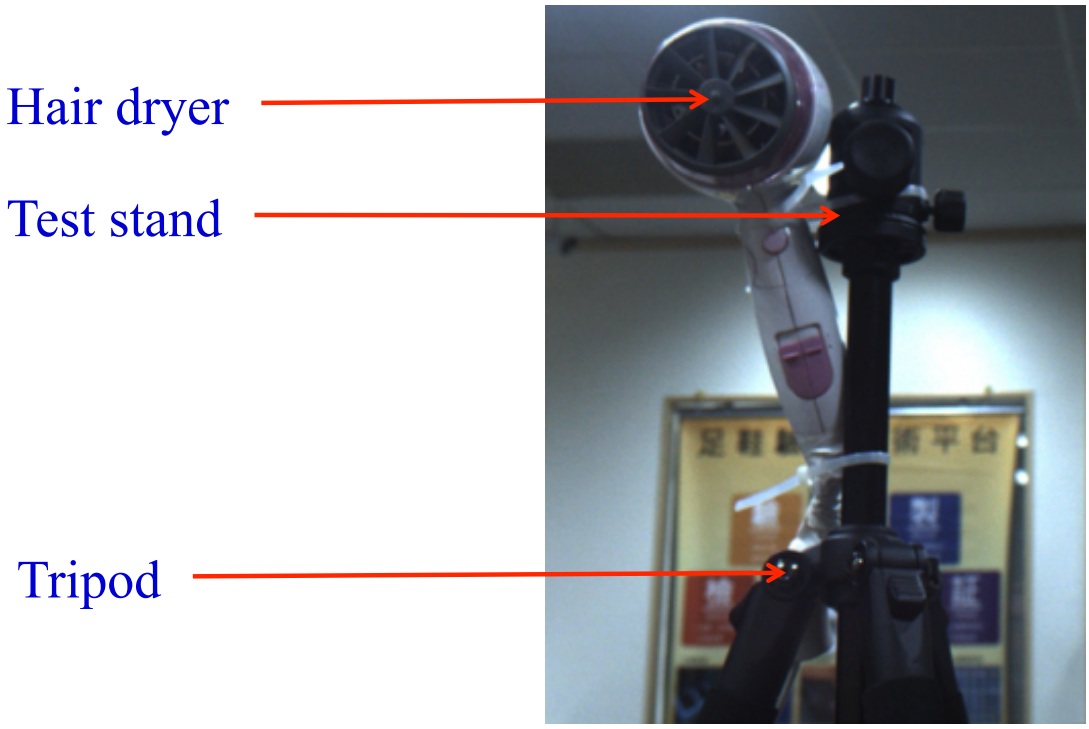

Figure 3. The test setup for studying the aerodynamically generated sound source and field resulting from a typical hair dryer under a non-ideal setting.

IV. Experimental Validations

First, we discuss the noise diagnosis and analysis results for a loudspeaker. Figures 4 to 8 show the results of using TSF V-Sonics to pinpoint the locations from which sounds were emitted from the loudspeaker, the reconstructed sound pressure distributions on the speaker surface and in 3D space, and intensity vector distributions on the loudspeaker surface in different frequency bands.

These results demonstrate that:

1. The proposed TSF V-Sonics technologies enable one to identify the locations from which sounds are emitted with very high spatial resolution, much less than one wavelength.
2. The number of sound sources that TSF V-Sonics can locate is much larger than the number of microphones involved.
3. TSF V-Sonics enables one to identify the relative source strengths on the source surfaces, which are directly responsible for sound radiation into the far field.
4. TSF V-Sonics enables one to see the radiation patterns in 3D space based on the identified sound sources.
5. TSF V-Sonics enables one to visualize the flow of acoustic energy from the source surface into the surrounding fluid medium, which indicates the locations and strengths of acoustic sources.
6. The SPL values on the loudspeaker surface are much higher than on other surfaces, which is confirmed in Figure 5.
7. The radiation patterns and characteristics revealed by the TSF V-Sonics technologies seem to be consistent with the sound source as expected. For example, a loudspeaker is expected to project sound toward the front, which is confirmed by a directional radiation pattern as shown in Figure 6.
8. The acoustic intensity vector distributions that indicate the strengths of the acoustic energy flows in different frequency bands from the source surface and supporting surfaces seem to be consistent with the expected results. For example, the majority of the acoustic energy is generated by the speaker, not supporting structure, which is confirmed in Figures 7 and 8.

Note that in this study, we have independently validated the locations where sounds were emitted by a given source. These results omitted here for brevity.

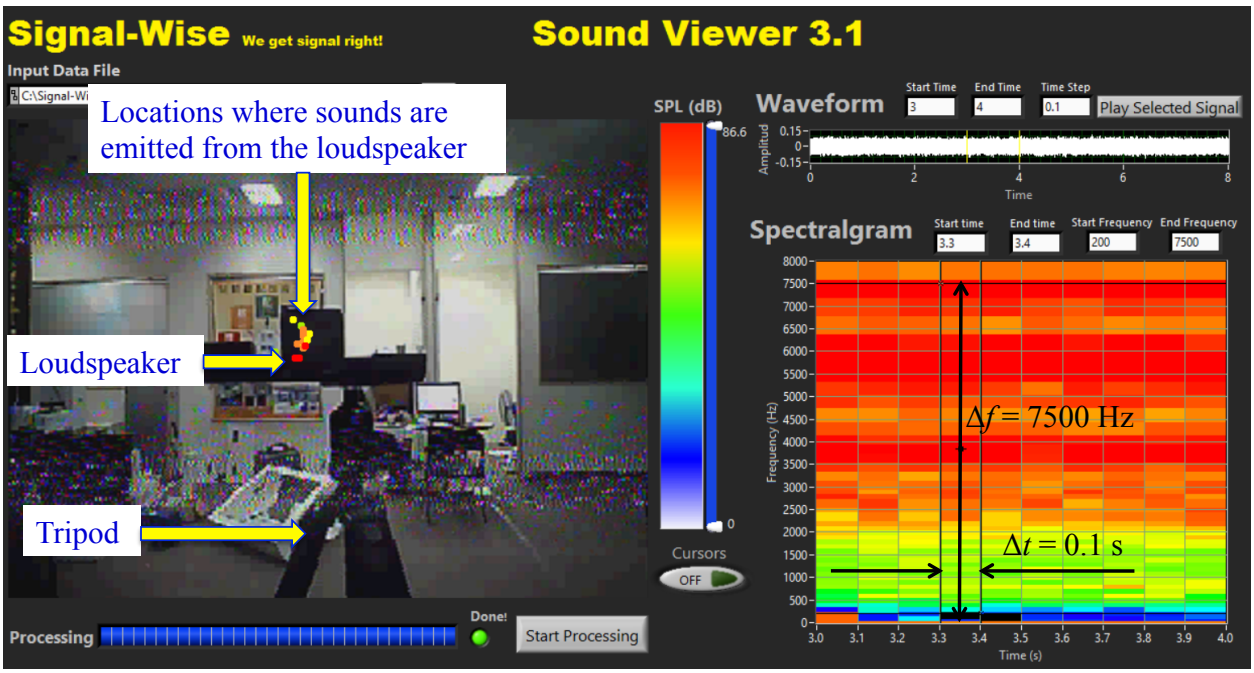

Figure 4. The identified locations where sounds were emitted from the loudspeaker over 0 – 7500 Hz frequency range and t = 3.3 – 3.4 sec. time step. The spatial resolution provided by TSF V-Sonics is very high and colors on the dots indicate the SPL (dB) values at the locations where sounds were emitted.

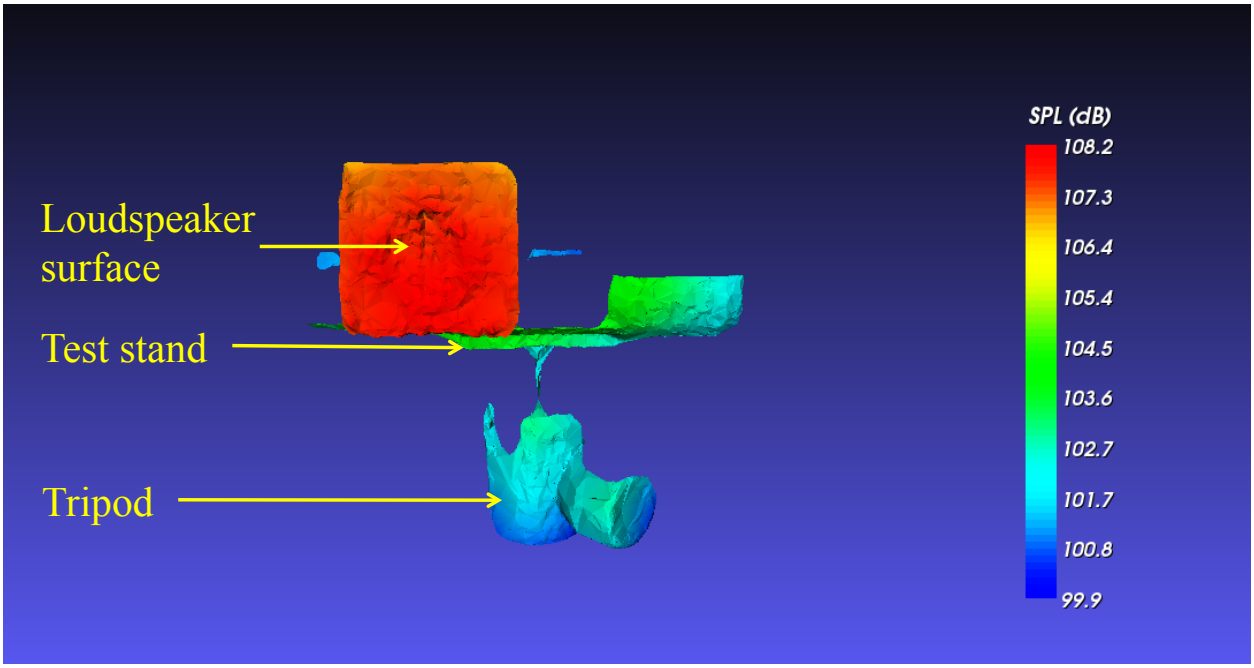

Figure 5. SPL value (dB) distributions on the loudspeaker surface and supporting structure surfaces over 0 – 7500 Hz frequency range and t = 3.3 – 3.4 sec. time step. Note that the SPL values distributions indicate relative contributions of acoustic radiation from this loudspeaker to the far field. They were not the actual SPL values of the loudspeaker that consisted of both the near- and far-field effects of an acoustic source.

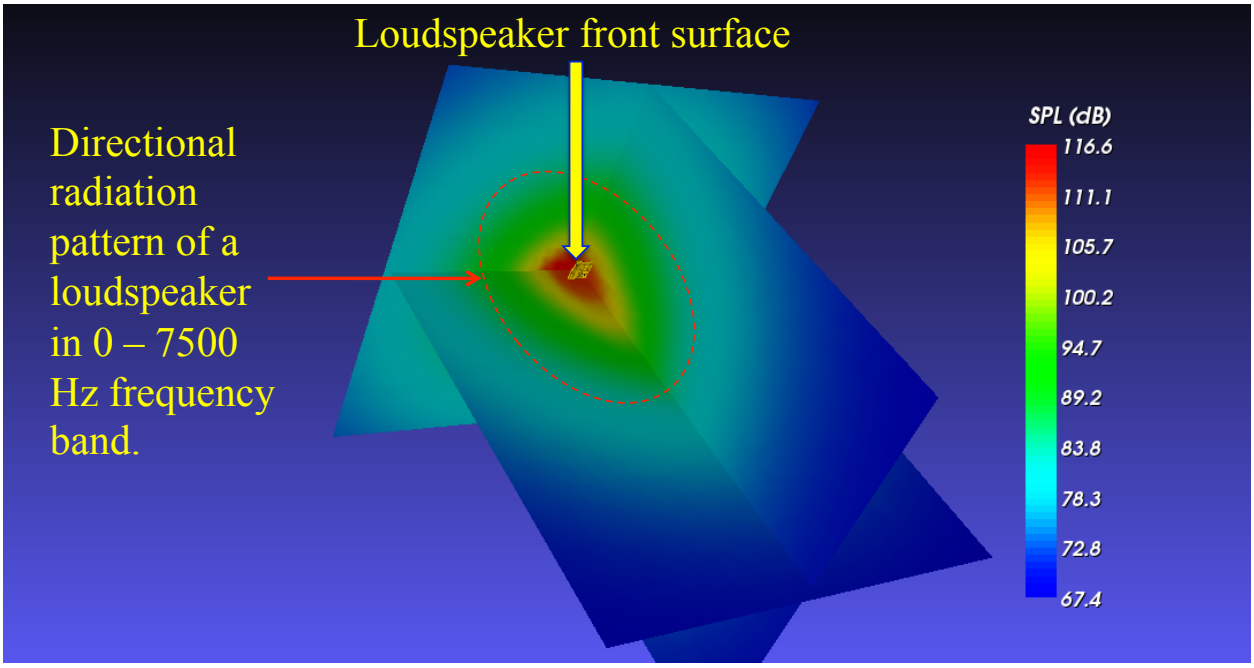

Figure 6. The radiation pattern of the loudspeaker over 0 – 7500 Hz frequency range, and $t = 3.3 – 3.4$ sec. time step. This radiation pattern seems consistent with the fact that a loudspeaker projects sound in the forward direction.

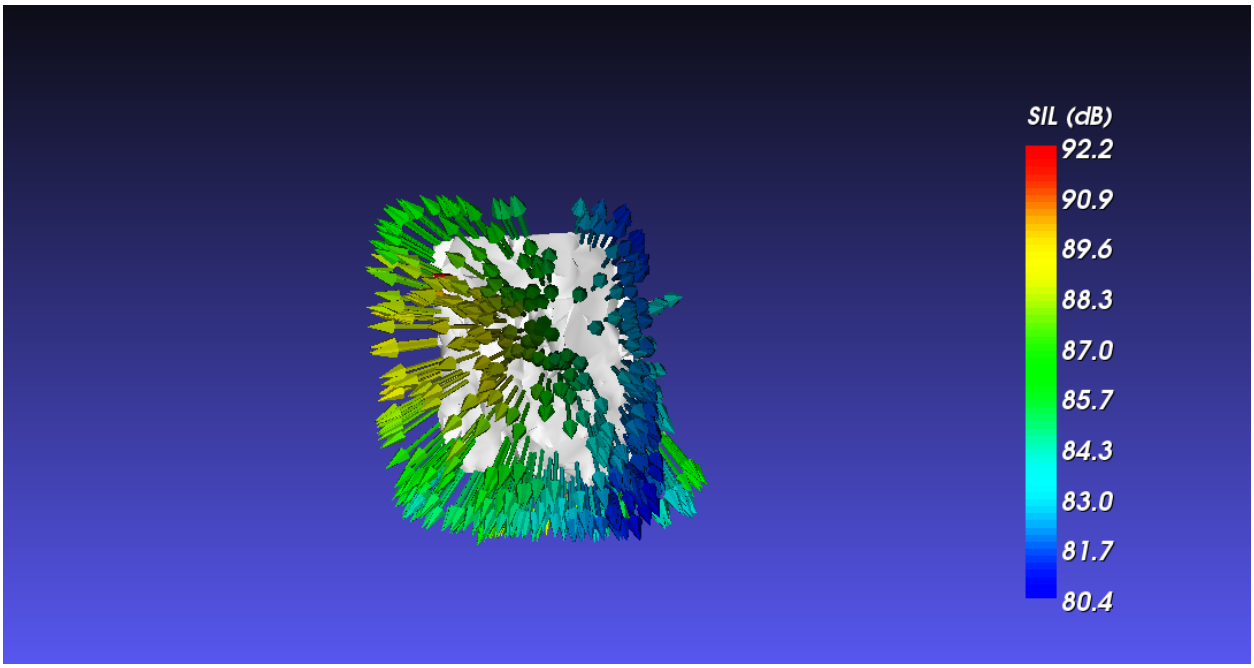

Figure 7. The acoustic intensity vector distribution on the surface of a loudspeaker over 0 – 2500 Hz frequency range and $t = 3.3 – 3.4$ sec. time step. Results clearly show the locations from which the acoustic energy is flowing out of the loudspeaker into the surrounding fluid medium. These acoustic intensities represent the far-field components that are responsible for acoustic radiation.

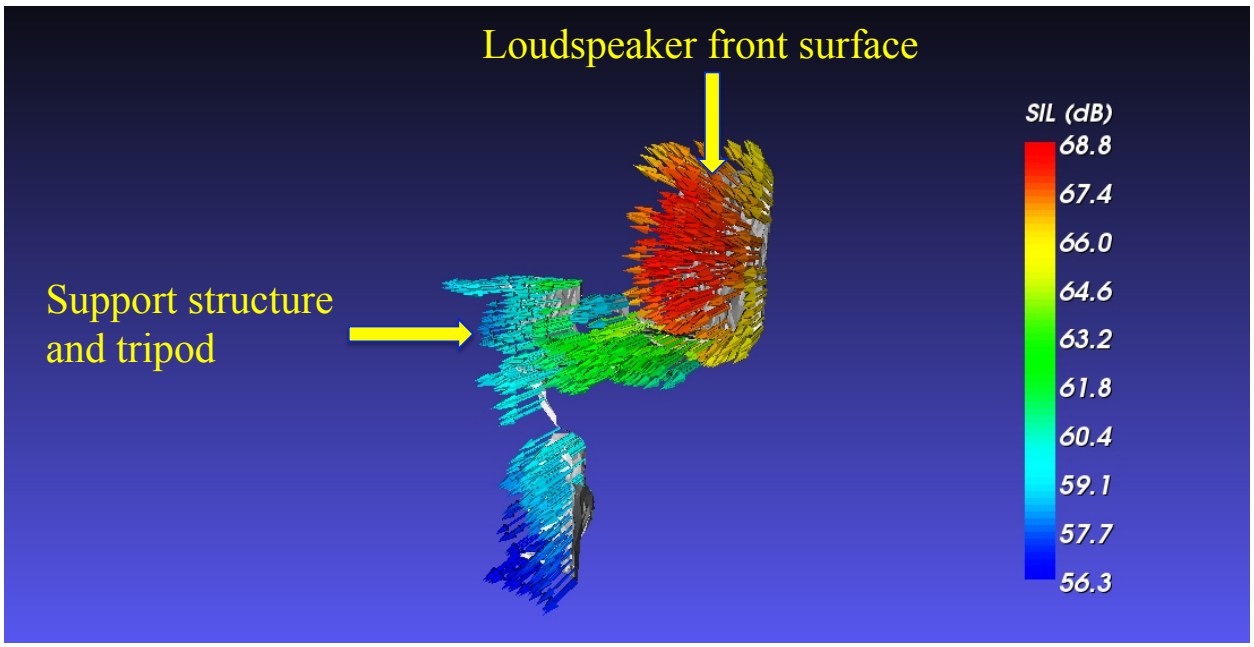

Figure 8. The acoustic intensity vector distributions on the loudspeaker surface and surfaces of supporting structures over 5000 – 7500 Hz frequency range and t = 3.3 – 3.4 sec. time step. Results confirm the fact that the acoustic energy is primarily generated by the loudspeaker itself, whereas those from the supporting structures are very small. Once again, these acoustic intensities represent the far-field components that are responsible for acoustic radiation.

Next, we discuss the results of using TSF V-Sonics to locate and analyze aerodynamically generated sound. Such a study is of significance in that it enables one to see the aerodynamically generated sound for the first time in terms of the source strengths on the surface and in 3D space. Most importantly, it offers a methodology and cost-effective tool for engineers to tackle various complex aerodynamically generated sound problems encountered in virtually any environment.

Figure 9 shows the locations from which aerodynamically generated sounds were emitted from a hair dryer. It is emphasized that these locations were not necessarily on the surface of a hair dryer, but in the downstream of the turbulent flow from the outlet of the hair dryer. These results seem consistent with aerodynamically generated sounds by turbulent flows in general. Once again, the spatial resolution of TSF V-Sonics is very high. The color scale indicates indicate the relative source strengths. Note that the SPL values represent the far-field components that are responsible for sound radiation into the far field.

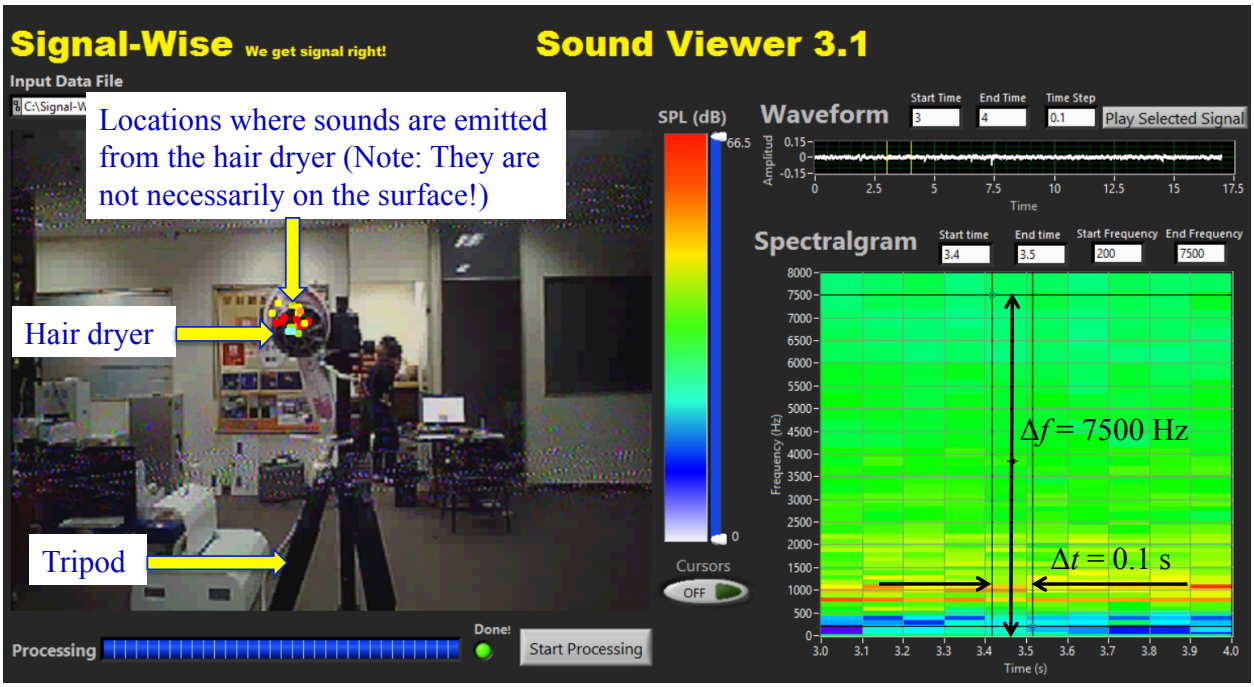

Figure 9. The locations from which aerodynamically generated sounds were generated over 0 – 7500 Hz frequency range and t = 3.4 – 3.5 sec. time step. The spatial resolution provided by TSF V-Sonics is very high and colors on the dots indicate the SPL (dB) values at the locations where sounds were emitted.

Figure 10 displays the corresponding sound radiation pattern over 0 – 7500 Hz frequency range and t = 3.4 – 3.5 sec. time step. Results correctly identified the major noise source of a hair dryer, namely, the blower between the inlet and outlet. Also, the radiation pattern of the turbulent flow in the downstream of the outlet of the hair dryer is clearly visualized.

Figure 11 exhibits the distribution of the acoustic intensity vectors on the surface of a hair dryer over 0 – 7500 Hz frequency range and t = 3.4 – 3.5 sec. time step. The strongest sound was emitted by the blower of the hair dryer, which was consistent with what we have often observed in practice. The second major sound was emitted from the outlet of the hair dryer as we have always observed in a hair dryer.

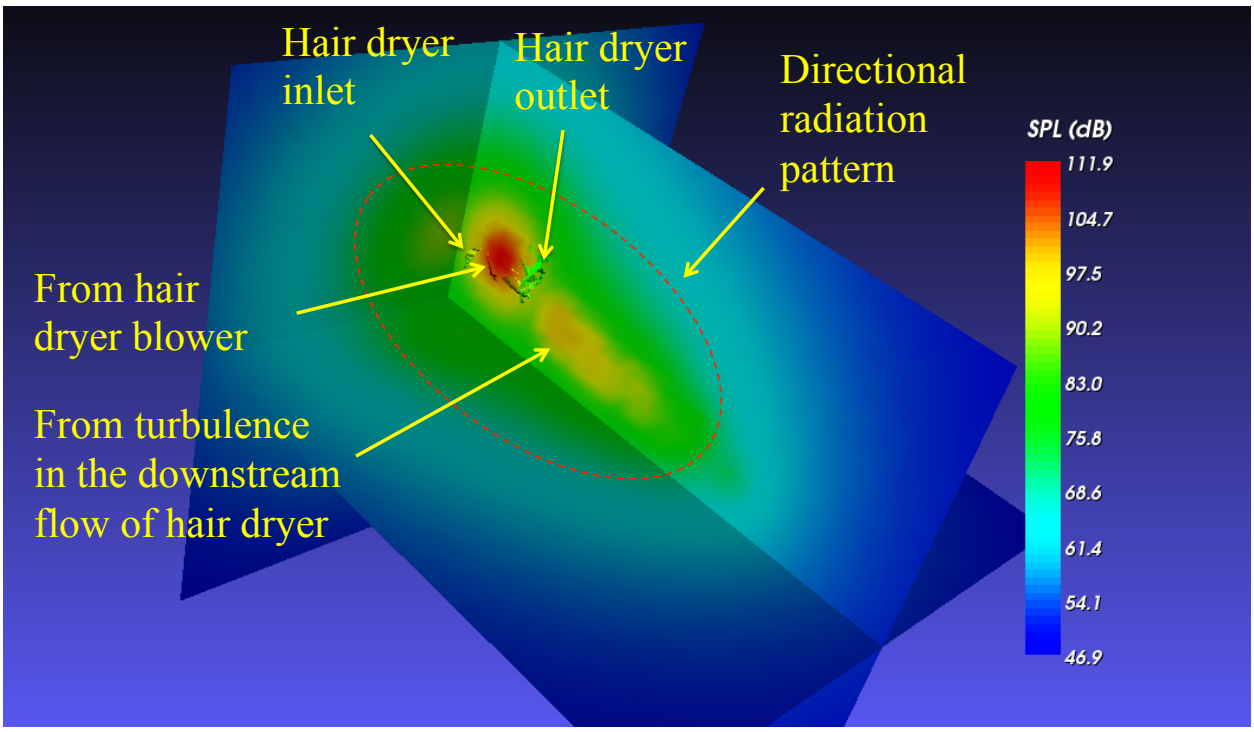

Figure 10. The radiation pattern of a hair dryer over 0 – 7500 Hz frequency range and t = 3.4 – 3.5 sec. time step. The major sound of a hair dryer was generated by the blower between the inlet and outlet, which confirmed what have always been observed in practice. Also shown is the radiation directivity due to turbulent flow in the downstream of the outlet of a hair dryer.

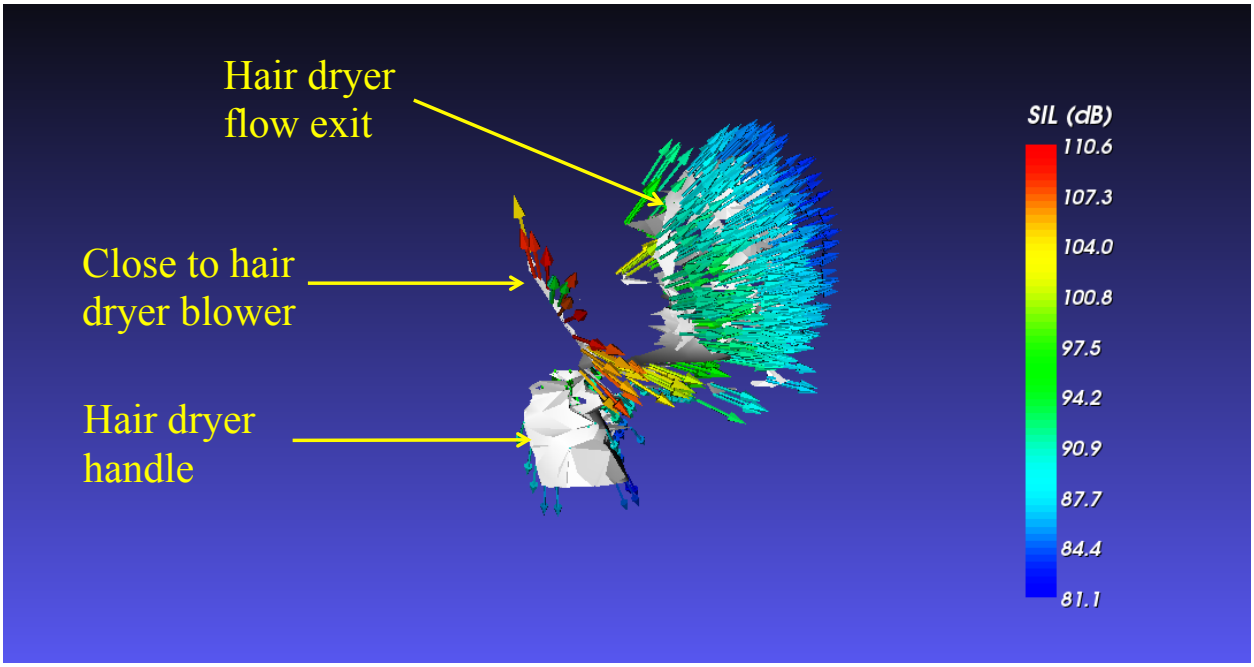

Figure 11. The acoustic intensity vector distributions on the surfaces of the hair dryer over 5000 – 7500 Hz frequency range and t = 3.4 – 3.5 sec. time step. Results confirmed the fact that the acoustic energy was primarily produced by the blower between the inlet and outlet of a hair dryer. The second major noise source was at the outlet of a hair dryer.

V. Conclusion

This study demonstrates that TSF V-Sonics can be used to locate and analyze a variety of complex noise sources in highly non-ideal environment. This is important because in practice the test conditions are non-ideal, involving an unknown number of reflecting surfaces and boundaries with vastly different acoustic absorption coefficients.

Specifically, test results confirm that:

1. TSF V-Sonics enables us to perform completely blind sound source localization and sound visualizations, including the aerodynamically generated sound sources and sound fields.
2. TSF V-Sonics can locate much more sound sources S than the number of microphones N ($S >> N$).
3. TSF V-Sonics can discriminate sound sources with very high spatial resolution, much less than one wavelength.
4. TSF V-Sonics is suitable for analyzing sound sources over a very wide frequency range.
5. TSF V-Sonics can offer these salient advantages with very few number of microphones.

References:

[1] J. Meyer, "Beamforming for a circular microphone array mounted on spherically shaped objects," *Journal of the Acoustical Society of America*, Vol. 109, 185 – 193 (2001).

[2] T. Tiana-Roig, F. Jacobsen, and E. Fernández Grande, "Beamforming with a circular microphone array for localization of environmental noise sources," *Journal of the Acoustical Society of America*, Vol. 128, 3535 – 3542 (2010).

[3] C. Bouchard, D. I. Havelock, and M. Bouchard, "Beamforming with microphone arrays for directional sources," *Journal of the Acoustical Society of America*, Vol. 125, 2098 – 2104 (2009).

[4] C. Bouchard, D. I. Havelock, and M. Bouchard, "Beamforming for directional sources: Additional estimator and evaluation of performance under different acoustic scenarios," *Journal of the Acoustical Society of America*, Vol. 129, 2042 – 2051 (2011).

[5] S. F. Wu and N. Zhu, "Passive sonic detection and ranging for locating arbitrary sound sources," *Journal of the Acoustical Society of America*, 133, 4054 – 404 (2013).

[6] S. F. Wu and N. Zhu, "Locating arbitrarily time-dependent sound sources in 3D space in real time," *Journal of the Acoustical Society of America*, 128, 728 – 739 (2010).

[7] N. Zhu and S. F. Wu, "Sound source localization in three-dimensional space in real time with redundancy checks," *Journal of Computational Acoustics*, 20, 125007-1 to 125007-16 (2012).

[8] S. F. Wu, *The Helmholtz Equation Least Squares Method for Reconstructing and Predicting Acoustic Radiation* (Springer, New York, 2015).

[9] S. F. Wu, "Methods for reconstructing acoustic quantities based on acoustic pressure measurements," *Journal of the Acoustical Society of America*, 124, 2680 – 2697 (2008).

[10] V. Isakov and S. F. Wu, "On theory and applications of the HELS method in inverse acoustics," Inverse Problem, **18**, 1147 – 1159 (2002).

[11] S. F. Wu, "Reconstructing transient acoustic radiation from an arbitrary object with a uniform surface velocity distribution," *Journal of the Acoustical Society of America*, 136, 514 – 524 (2014).

[12] S. F. Wu, M. Moondra, and R. Beniwal, "Analyzing panel acoustic contributions toward the sound field inside the passenger compartment of a full-size automobile," *Journal of the Acoustical Society of America*, 137, 2101 –2112 (2015).